Article
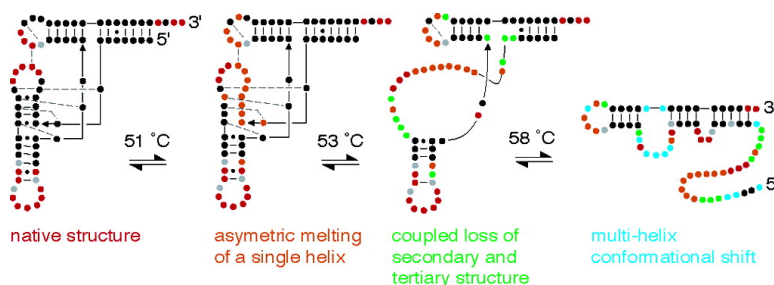
RNA SHAPE Chemistry Reveals Nonhierarchical Interactions Dominate Equilibrium Structural Transitions in tRNA Transcripts

Kevin A. Wilkinson, Edward J. Merino, and Kevin M. Weeks

native structure | asymetric melting of a single helix | coupled loss of secondary and tertiary structure | multi-helix conformational shift

More About This Article

Additional resources and features associated with this article are available within the HTML version:

- Supporting Information
- Links to the 9 articles that cite this article, as of the time of this article download
- Access to high resolution figures
- Links to articles and content related to this article
- Copyright permission to reproduce figures and/or text from this article

View the Full Text HTML

RNA SHAPE Chemistry Reveals Nonhierarchical Interactions Dominate Equilibrium Structural Transitions in tRNA^Asp Transcripts

Kevin A. Wilkinson, Edward J. Merino, and Kevin M. Weeks*

Contribution from the Department of Chemistry, University of North Carolina, Chapel Hill, North Carolina 27599-3290

Received October 18, 2004; E-mail: weeks@unc.edu

Abstract: Current models assume that RNA folding is strongly hierarchical such that the base-paired secondary structure is more stable than and forms independently of the tertiary structure. This model has been difficult to test due to the experimental inability to interrogate the local environment at every nucleotide as a comprehensive function of the RNA folding state. Reaction of an RNA 2′-hydroxyl group with *N*-methylisatoic anhydride to form a nucleotide 2′-ester is governed by the extent to which the nucleotide forms base pairing or tertiary interactions. Selective 2′-Hydroxyl Acylation analyzed by Primer Extension (SHAPE) is shown to be an RNA analogue of the protein hydrogen exchange experiment. Single nucleotide resolution SHAPE analysis emphasizes a complexity for the unfolding of tRNA^Asp transcripts that is not anticipated by current models for RNA folding. We quantify six well-defined transitions for tRNA^Asp transcripts between 35 and >75 °C, including asymmetric unfolding of the two strands in a single helix, multistep loss of tertiary interactions, and a multihelix conformational shift. The three lowest temperature transitions each involve coupled interactions between the secondary and tertiary structure. Thus, even for this simple RNA, multiple nonhierarchical and complex interactions dominate the equilibrium transitions most accessible from the native state.

Introduction

Essentially all RNA molecules undergo a unimolecular folding reaction to form extensive interactions that locally constrain nucleotides in base-paired secondary structures and, often, in long-range tertiary interactions.[1,2] Nucleotides in folded RNAs thus differ significantly in the extent to which they are conformationally restrained by interactions with other parts of an RNA. Despite well documented exceptions,[3] current models for RNA folding and for de novo prediction of RNA structure emphasize that RNA folding is strongly hierarchical. Hierarchical folding means that the base-paired secondary structure both is more stable than and forms independently of the tertiary structure. The hierarchical model has been difficult to test thoroughly because it has not been possible to experimentally evaluate folding states at nucleotide resolution for large RNAs. Nucleotide resolution is essential because functionally important helices often span only a few base pairs[2] and many important tertiary interactions in RNA involve only one or a few nucleotides.[4] In the protein folding world, local residue dynamics are elegantly monitored in backbone amide hydrogen exchange experiments.[5,6] A similarly comprehensive and nucleotide

resolution experiment has not been developed for analysis of RNA structure and RNA folding intermediates.

The ribose 2′-hydroxyl group reacts with *N*-methylisatoic anhydride (NMIA) to form ester adducts at the 2′ position.[7,8] The reactivity of the 2′-hydroxyl group is gated by the underlying local structure such that flexible nucleotides react to form a 2′-O-adduct more readily than nucleotides constrained by base pairing or tertiary interactions,[7] as illustrated in eq 1:

$$(RNA)_{constrained} \underset{k_c}{\overset{k_f}{\rightleftharpoons}} (RNA)_{flexible} \xrightarrow[CO_2]{k_2 [NMIA]} RNA \quad (1)$$
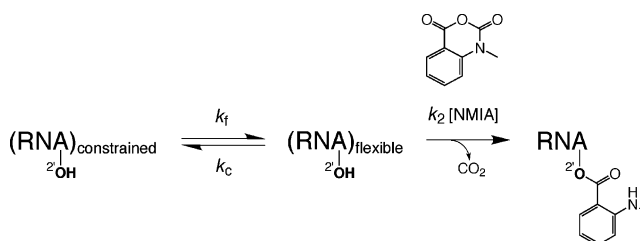
2′-Hydroxyl reactivity scores local nucleotide flexibility because unconstrained nucleotides are better able to adopt an open conformation in which formation of a 2′-oxyanion nucleophile is less destabilized by the adjacent 3′-phosphodiester anion.[7] Under our standard conditions, 2′-ester formation with NMIA (the pseudo-first-order k_2[NMIA] step) occurs at a rate of 0.02 min^{-1} at highly reactive 2′-hydroxyl positions. This rate is many orders of magnitude slower than the rate constants for

(1) (a) Brion, P.; Westhof, E. *Annu. Rev. Biophys. Biomol. Struct.* **1997**, *26*, 113−137. (b) Tinoco, I.; Bustamante, C. *J. Mol. Biol.* **1999**, *293*, 271−281.
(2) Gesteland, R. F.; Cech, T. R.; Atkins, J. F. *The RNA World*, 2 ed.; Cold Spring Harbor Laboratory Press: Cold Spring Harbor, 1999.
(3) (a) LeCuyer, K. A.; Crothers, D. M. *Biochemistry* **1993**, *32*, 5301−5311. (b) Gluick, T. C.; Draper, D. E. *J. Mol. Biol.* **1994**, *241*, 246−262. (c) Wu, M.; Tinoco, I. *Proc. Natl. Acad. Sci. U.S.A.* **1998**, *95*, 11555−11560.
(4) (a) Levitt, M. *Nature* **1969**, *224*, 759−763. (b) Nissen, P.; Ippolito, J. A.; Ban, N.; Moore, P. B.; Steitz, T. A. *Proc. Natl. Acad. Sci. U.S.A.* **2001**, *98*, 4899−4903. (c) Leontis, N. B.; Stombaugh, J.; Westhof, E. *Nucleic Acids Res.* **2002**, *30*, 3497−3531.

(5) Englander, S. W.; Kallenbach, N. R. *Q. Rev. Biophys.* **1983**, *16*, 521−655.
(6) Englander, S. W. *Annu. Rev. Biophys. Biomol. Struct.* **2000**, *29*, 213−238.
(7) Merino, E. J.; Wilkinson, K. A.; Coughlan, J. L.; Weeks, K. M. *J. Am. Chem. Soc.* **2005**, *127*, accepted for publication.
(8) (a) Moorman, A. R.; Abeles, R. H. *J. Am. Chem. Soc.* **1982**, *104*, 6785−6786. (b) Hiratsuka, T. *Biochim. Biophys. Acta* **1983**, *742*, 496−508.

base-pair opening,[5,9] base flipping,[10] or local base destacking[11] processes, represented by the rate constants k_f and k_c in eq 1. Studies with model compounds also indicate that flexible nucleotides react ~5–30-fold more slowly than nucleotide analogues specifically designed to reduce inhibition of the 2′-O-adduct-forming reaction by the adjacent 3′-phosphodiester.[7] Thus, the equilibrium constant, represented by the ratio k_f/k_c, is less than 1, even for reactive, single-stranded positions. The rate constant for 2′-adduct formation, k_{adduct}, is therefore determined by the fraction of time a nucleotide exists in the unconstrained, reactive conformation, multiplied by the rate of the chemical transformation:

$$k_{adduct} = K_f \, k_2 [\text{NMIA}] \qquad (2)$$

where $K_f = k_f/k_c$ and with the proviso that [NMIA] decreases during the reaction due to hydrolysis.[7] A significant, perhaps counterintuitive, bonus of NMIA chemistry is that this reagent degrades by competitive hydrolysis with water,[7] which we will show means that RNA structure can be monitored without the requirement that temperature-dependent reaction parameters be carefully controlled.

Selective 2′-hydroxyl acylation thus represents an RNA analogue of the widely employed protein amide hydrogen exchange[5,6] experiment in the bimolecular (EX2) limit. Because k_2[NMIA] is slow, NMIA-based interrogation of RNA folding states is restricted to analysis of folding intermediates at equilibrium. Each nucleotide in an RNA cycles through all possible states, including unfolded states, weighted by the Boltzmann distribution. Flexible nucleotides will populate a different distribution of conformations than base paired or constrained positions. The conformation that most facilitates 2′-O-adduct formation will dominate relative reactivity at any given position, and flexible nucleotides will more often sample the most reactive conformations.[7] Because all ribonucleotides have a 2′-hydroxyl, absent a few with post-transcriptional modifications at this position,[12] structural information is, in principle, obtainable for every nucleotide in an RNA.

The entire structure-sensitive experiment involves selective 2′-hydroxyl acylation (eq 1) and analysis of sites of 2′-O-adduct formation by primer extension (SHAPE). In this work, we use RNA SHAPE mapping to analyze unfolding profiles for yeast tRNA^{Asp} transcripts with simultaneous interrogation of the local structural environment at almost every nucleotide. Even for this relatively simple and well-studied RNA,[7,13–15] SHAPE analysis reveals a pathway for unfolding intermediates that is significantly richer and more detailed than previously observable. The most thermally accessible states involve strong and nonhierarchical linkages between disparate elements of the tRNA structure.

Results

**NMIA Modification Proceeds to Identical Endpoints, Independent of Temperature.** *N*-Methylisatoic anhydride

(9) Snoussi, K.; Leroy, J.-L. *Biochemistry* **2001**, *40*, 8898–8904.
(10) Spies, M. A.; Schowen, R. L. *J. Am. Chem. Soc.* **2002**, *124*, 14049–14053.
(11) Jean, J. M.; Hall, K. B. *Biochemistry* **2004**, *43*, 10277–10284.
(12) (a) Decatur, W. A.; Fournier, M. J. *J. Biol. Chem.* **2003**, *278*, 695–698. (b) Agris, P. F. *Nucleic Acids Res.* **2004**, *32*, 223–238.
(13) (a) Westhof, E.; Dumas, P.; Moras, D. *J. Mol. Biol.* **1985**, *184*, 119–145. (b) Westhof, E.; Dumas, P.; Moras, D. *Acta Crystallogr. A* **1988**, *44*, 112–123.
(14) (a) Romby, P.; Moras, D.; Dumas, P.; Ebel, J. P.; Giege, R. *J. Mol. Biol.* **1987**, *195*, 193–204. (b) Perret, V.; Garcia, A.; Puglisi, J.; Grosjean, H.; Ebel, J. P.; Florentz, C.; Giege, R. *Biochimie* **1990**, *72*, 735–743.
(15) Chamberlin, S. I.; Weeks, K. M. *J. Am. Chem. Soc.* **2000**, *122*, 216–224.
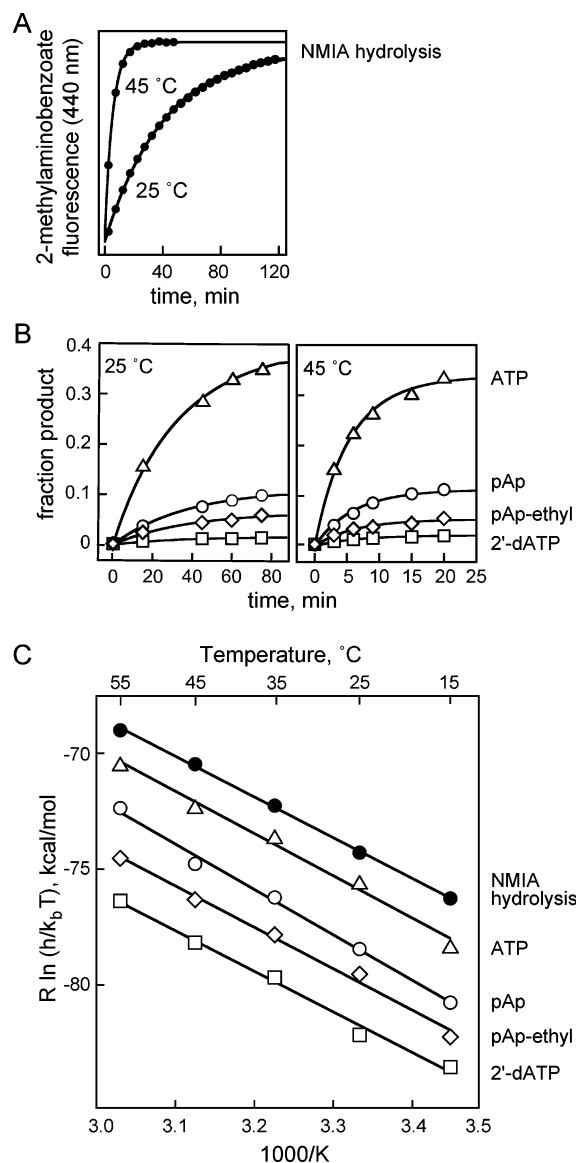
Figure 1. 2′-O-adduct-forming potential of NMIA is independent of temperature. (A) Representative NMIA hydrolysis profiles, monitored by formation of the fluorescent 2-methylaminobenzoate product. Measured hydrolysis rate constants for NMIA at 15, 25, 35, 45, and 55 °C are 0.009, 0.031, 0.071, 0.179, and 0.385 min^{-1}, respectively. (B) Reaction profiles for nucleotide analogues with a broad range of intrinsic 2′-hydroxyl reactivities. For clarity, the *x*-axes span different time domains in the 25 and 45 °C panels. ATP, pAp, pAp-ethyl, and 2′-deoxy-ATP are adenosine 5′-triphosphate, 5′,3′-bisadenosine diphosphate, 3′-phosphoethyl-5′-adenosine monophosphate, and 2′-deoxy-adenosine triphosphate, respectively. (C) Eyring analysis of NMIA hydrolysis (solid circles) and of nucleotide 2′-O-adduct formation (open symbols) indicates that rates increase, quantitatively, in parallel. Slopes shown give $\Delta H^{\ddagger}$ directly, which is 19(±2) kcal/mol for all reactions.

(NMIA) reacts both with nucleotides to form the 2′-O-adduct (eq 1) and with water to degrade to 2-methylaminobenzoate.[7] To use selective 2′-ester formation to map folding transitions in RNA as a function of temperature, we needed to understand how NMIA hydrolysis and nucleotide reactivity change with this variable.

We determined the rate constant for NMIA hydrolysis by monitoring formation of the fluorescent 2-methylaminobenzoate product (Figure 1A); hydrolysis rate constants show linear Eyring behavior (solid symbols in Figure 1C). We monitored formation of the 2′-*O*-methylaminobenzoyl adduct using four
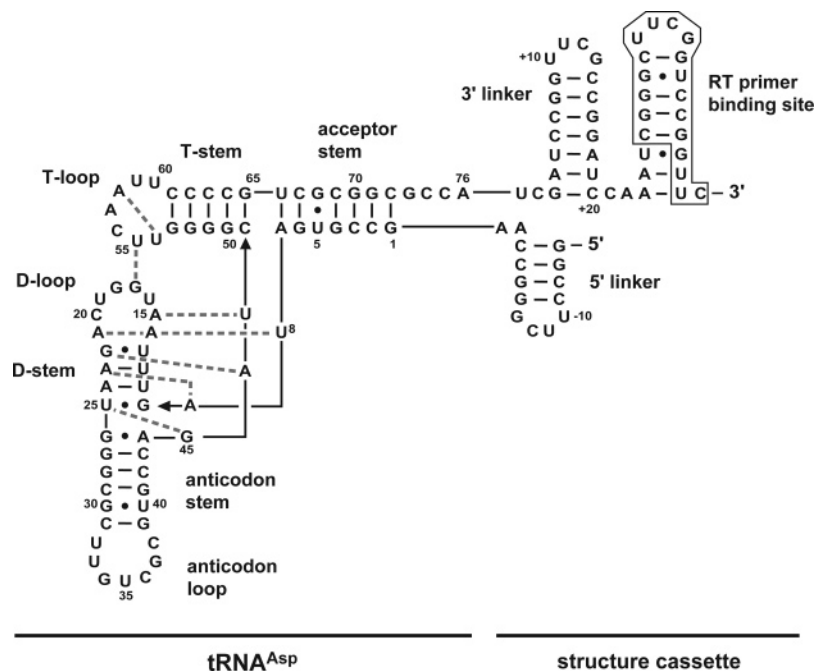
Figure 2. The tRNA^Asp transcript in the context of an RNA structure cassette; tRNA^Asp structure is drawn to suggest orientation of helices and tertiary interactions in three-dimensional space. Tertiary interactions are indicated by dashed lines in gray. The 5′ and 3′ linker regions facilitate analysis of sites of 2′-O-adduct formation by primer extension and have been shown to fold independently of the internal tRNA structure.[7] By convention,[13] nucleotides in yeast tRNA^Asp are numbered 1−76, with residue 47 omitted.

nucleotide analogues: ATP, pAp, pAp-ethyl, and 2′-deoxy-ATP (Figure 1B). The pAp-ethyl represents a good analogue for unstructured RNA,[7] while the other analogues span a broad range of rates for 2′-O-adduct formation with NMIA. While the absolute rate constant for each nucleotide increased by ∼5-fold as the temperature increased from 25 to 45 °C, the fraction 2′-O-adduct formed at long time points is identical, within error, at all temperatures (Figure 1B). All four analogues also show linear behavior in an Eyring plot (open symbols, Figure 1C), and all rates show an activation enthalpy of 19 ± 2 kcal/mol.

These experiments provide two fundamental insights. First, NMIA degrades on an experimentally tractable time scale (hydrolysis half-life ≈ 11 min at 35 °C), and thus RNA structure probing (eq 1) can be performed without an explicit reagent quenching step. It is sufficient instead simply to allow RNA modification to proceed for five hydrolysis half-lives. Second, because all slopes in the Eyring plot are parallel (Figure 1C) and because the fraction 2′-O-adduct formed at long times for each of the four nucleotide analogues is independent of temperature (compare endpoints in the 25 and 45 °C panels in Figure 1B), the absolute 2′-O-adduct-forming potential is *constant* for an RNA nucleotide that does not undergo a change in conformation. If NMIA degradation proceeds to completion, no reactivity correction for temperature is required.

Nucleotide Resolution Analysis of RNA Folding Intermediates. We used SHAPE to analyze thermally accessible states for yeast tRNA^Asp transcripts. Although this RNA does not contain the post-transcriptional modifications of the cellular RNA, extensive prior work shows that the unmodified version folds into the correct L-shaped tRNA structure[14] and is bound and aminoacylated by its cognate synthetase indistinguishably from the wild-type RNA.[16] The tRNA^Asp was synthesized in the context of an RNA structure cassette (Figure 2). This cassette embeds the tRNA within flanking 5′ and 3′ linker structures that facilitate detection of sites of 2′-O-adduct formation by

primer extension.[7] SHAPE analysis shows that the internal tRNA^Asp structure folds autonomously, and that the flanking hairpins fold independently, as designed.[7]

The structure of the tRNA^Asp construct was analyzed by SHAPE at temperatures spanning 35−75 °C in intervals of ≤3.5 °C (Figure 3, left-most 18 lanes). The RNA was treated with NMIA at each temperature under single hit conditions[7] until reagent degradation was 97% complete (five half-lives). Sites of 2′-O-adduct formation were mapped by primer extension. Strong stops to primer extension are not observed in control experiments omitting NMIA or in which NMIA was allowed to degrade prior to addition of RNA (compare −NMIA and prequench lanes with +NMIA reactions, Figure 3).

Overall banding patterns for the 18 independent experiments show clear differences that reflect secondary and tertiary interactions and smooth transitions as a function of temperature (Figure 3, structural landmarks are indicated at left). The SHAPE experiment accurately reports the canonical structure of tRNA^Asp at 35 °C and 10 mM MgCl$_2$ because all highly reactive nucleotides lie in loops in tRNA^Asp or the structure cassette. With increasing temperature, the tRNA^Asp transcript more readily forms 2′-O-adducts, consistent with increased local nucleotide flexibility in the RNA (Figure 3).

We quantified the folding state for almost every nucleotide in the RNA as a function of temperature. Band intensities were normalized to a unit scale to facilitate comparison between different nucleotides. We observed five distinct reactivity patterns (Figure 4). In the first group (Figure 4A), 10 positions, including all residues in the T-stem, remain unreactive at all temperatures (see 75 °C lane, Figure 3; summarized as filled stars in Figure 5). These residues correspond to positions that remain stably base paired below 75 °C.

(16) (a) Perret, V.; Garcia, A.; Grosjean, H.; Ebel, J. P.; Florentz, C.; Giege, R. *Nature* **1990**, *344*, 787−789. (b) Sissler, M.; Eriani, G.; Martin, F.; Giege, R.; Florentz, C. *Nucleic Acids Res.* **1997**, *25*, 4899−4906.
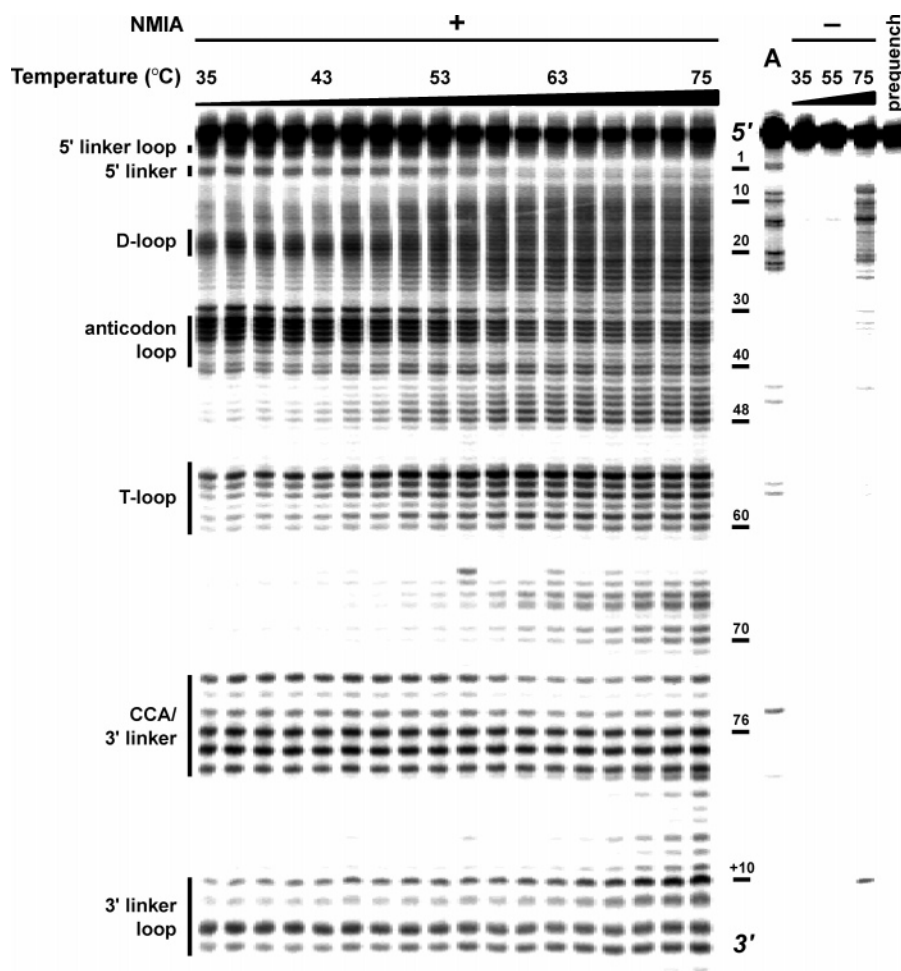
Figure 3. Temperature-dependent SHAPE analysis of tRNA^{Asp}. RNA structural landmarks are indicated at left. For the +NMIA reactions, bands correspond to stops in reverse transcriptase-mediated primer extension and report sites of 2′-O-adduct formation; −NMIA lanes omitted reagent. The dideoxy sequencing ladder (A) is offset exactly 1 nucleotide longer than the corresponding 2′-adduct bands; nucleotide positions are numbered relative to NMIA lanes. For the prequench lane, NMIA was added and allowed to degrade prior to addition of RNA.

In the second class (Figure 4B), 10 nucleotides in tRNA^{Asp} (G18, U19, C20, U33, G34, U35, G37, C38, C75, and A76) exhibit roughly uniform high reactivity at all temperatures. These nucleotides are located in the anticodon loop, in the D-loop, and at the 3′-CCA terminus and correspond precisely to flexible, unpaired regions (summarized as red circles in Figure 5).

For the third and fourth classes, many positions undergo well-behaved transitions in which 2′-hydroxyl reactivity changes smoothly between 35 and 75 °C. However, the tRNA^{Asp} construct does not unfold in a single transition or even in a few transitions. Instead, SHAPE quantitatively identifies a minimum of six structural transitions for tRNA^{Asp} spanning from ~50 to >70 °C (Figure 4A,D–H). Transition midpoints (melting temperatures, T_m) measured at each nucleotide are summarized in Figure 5. We group the observed transition midpoints by color, and this scheme is used consistently throughout this work.

Structures in the third class show relatively simple behavior in which reactivity increases from a low to a high value (see, for example, D-stem residues 10–13 and 22–25 in Figure 3), consistent with a monotonic transition from a structure constrained by base pairing or tertiary interactions to an unconstrained conformation (indicated by T_m in Figure 5).

In contrast, in the fourth class, several nucleotides located in the D- and T-loops are reactive at 35 °C but additionally exhibit clear unfolding transitions with increasing temperature (see

Figure 3; emphasized with a circled T_m in Figure 5). We infer that these are partially constrained positions that then experience greater conformational flexibility with increasing temperature.

Finally, three positions are initially reactive but have structural profiles that show complex two-phase transitions (for example, position G73 in Figure 3). At these nucleotides, 2′-hydroxyl reactivity first decreases and then increases (Figure 4C, diamonds in Figure 5). The net amplitude of the *reduction* in 2′-hydroxyl reactivity is comparable to that observed for the multiple, simple transitions in which reactivity *increases*. The observed, well-defined reductions and subsequent enhancements in reactivity are consistent with a model in which these nucleotides participate in new, constraining interactions at intermediate temperatures which are then destabilized with increasing temperature.

We were also able to monitor 2′-hydroxyl reactivity in significant portions of the 5′ and 3′ regions of the structure cassette (Figures 2 and 3). All of the nucleotides in the 5′ and 3′ linker loops are reactive, and all base-paired nucleotides in these structures show either no unfolding transition or an incomplete transition by 75 °C (comparable to the transitions shown in Figure 4A,D). Thus, helices in the structure cassette fold independently, as designed, and do not interfere with folding of the internal tRNA^{Asp}.

**Comparison of SHAPE with Absorbance-Detected Denaturation.** We compared the nucleotide resolution information
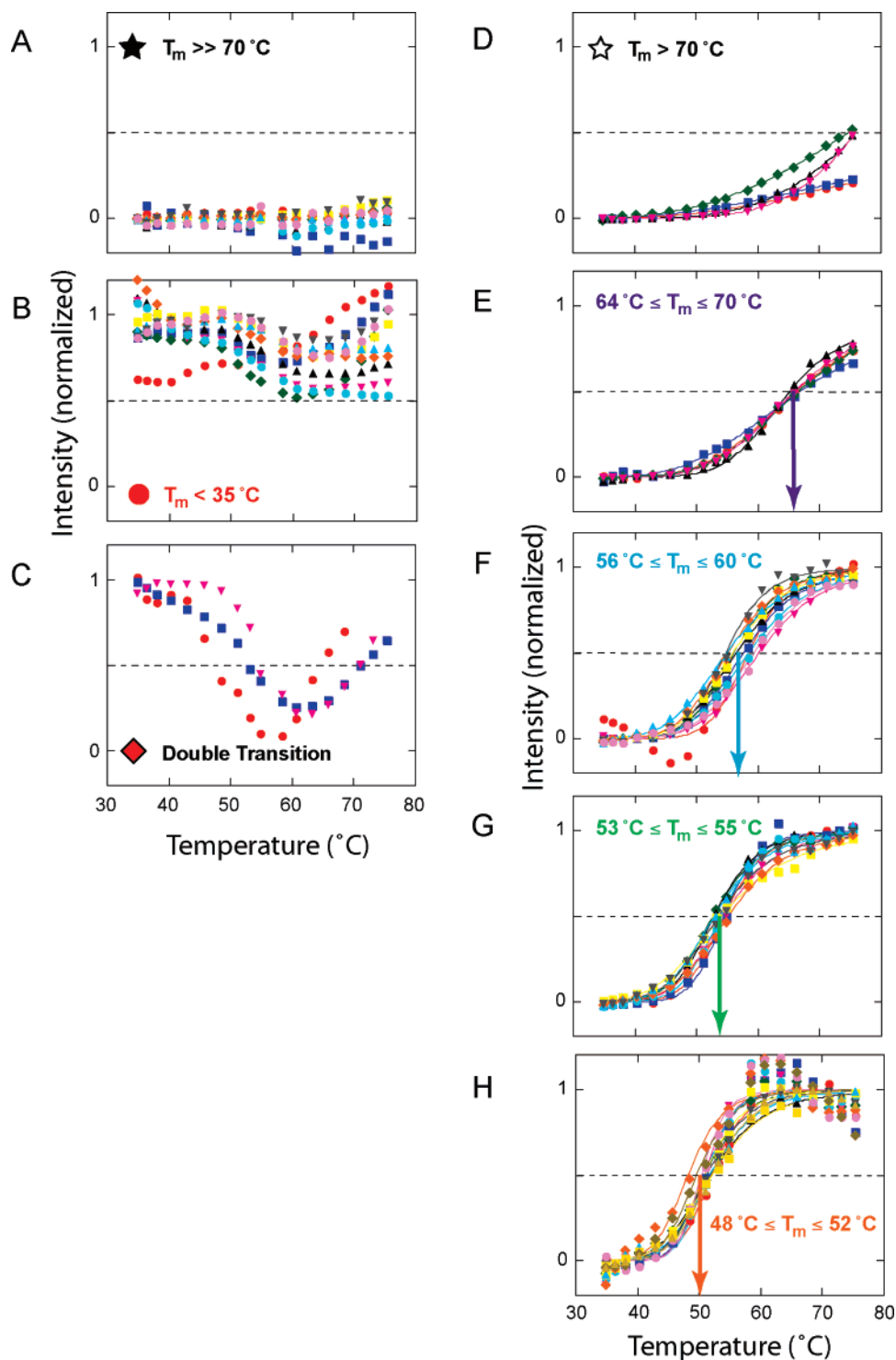
Figure 4. Single nucleotide unfolding profiles for tRNA^Asp. Profiles were computed by quantifying almost every band shown in Figure 3. (A–H) Profiles for each nucleotide binned by behavior. Data are plotted on a linear scale; dashed line indicates fraction melted = 0.5. Nucleotides with well-defined unfolding transitions (E–H) were fit to an equation assuming unimolecular denaturation and grouped according to T_m.

obtained by the SHAPE approach (Figure 4) with a conventional absorbance-detected experiment, performed under identical solution conditions (Figure 6). RNA absorbance in the ultraviolet region increases with temperature due to disruption of base-stacking interactions (open symbols, Figure 6). Global unfolding features are more readily visualized in a first derivative plot (solid symbols, Figure 6), which shows two broad denaturation transitions for the tRNA^Asp transcript spanning ~45–75 and 75–90 °C.

The SHAPE experiments agree well with the absorbance melting profile (transitions detected by SHAPE are emphasized in color in Figure 6). The transitions detected at 51 and 58 °C correspond to features (just barely) detectable in the absorbance melting experiment. The transition maximum seen in the first derivative plot of the absorbance melting experiment (~63 °C) does not correspond to a single RNA unfolding transition but, instead, appears to report a convolution of the SHAPE-detected transitions occurring at 58 and 66 °C (compare blue and magenta
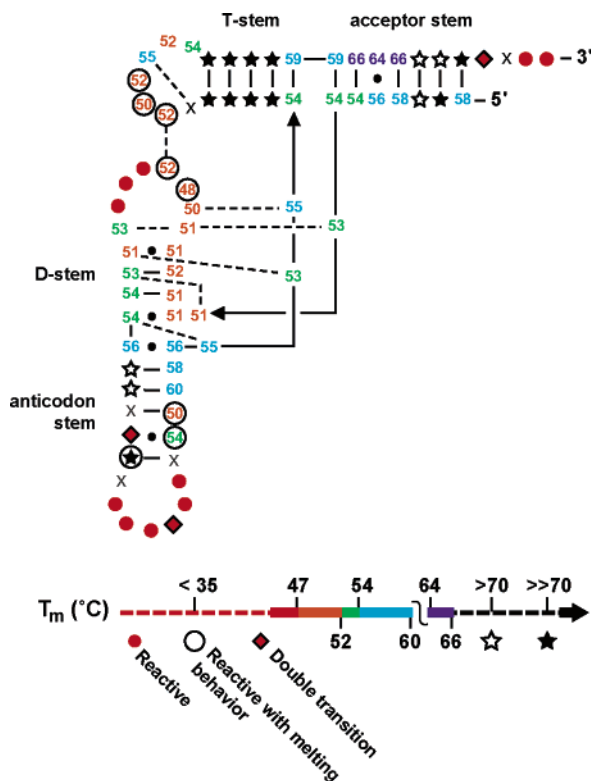
Figure 5. Summary of structural transitions at nucleotide resolution superimposed on a secondary structure for tRNA^{Asp}. Nucleotides are represented by their transition midpoint (T_m). Positions that have just begun to unfold at 70 °C or that unfold with a $T_m \gg$ 70 °C are shown with open and closed stars, respectively. Colors correspond to melting temperature scheme used in previous and subsequent figures. Positions C28, U32, G39, and U54 (*x*) could not be analyzed, either because of electrophoretic band compression[15] or because of absence of a reproducible profile.
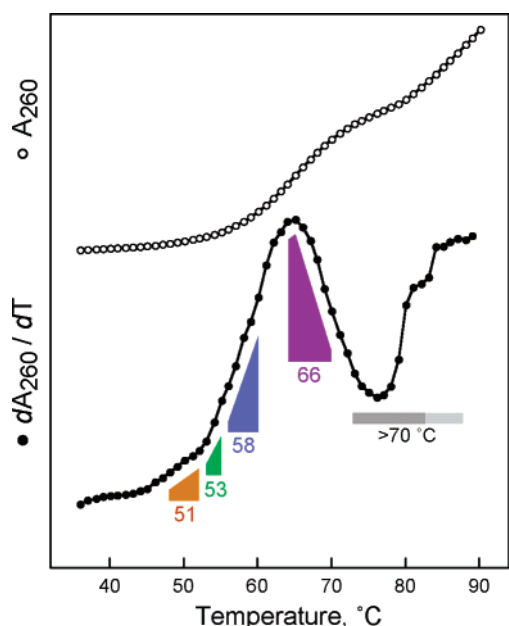
Figure 6. Absorbance melting profile of the tRNA^{Asp} transcript. Absorbance, monitored at 260 nm, and the first derivative with respect to temperature are shown with open and closed symbols, respectively. Nucleotide resolution transition ranges determined by SHAPE (Figure 4) are illustrated in color.

regions with solid symbols in Figure 6). In sum, RNA SHAPE mapping is quantitatively consistent with the bulk RNA absor-

bance melting experiment but uniquely yields structural information at nucleotide resolution.

Discussion

Model for the Unfolding Pathway of tRNA^{Asp} at Single Nucleotide Resolution. The nucleotide resolution SHAPE approach provides model-independent information on the local nucleotide environment in tRNA^{Asp} as a function of temperature (Figures 3−5). To interpret these data and to develop structural models for tRNA^{Asp} folding intermediates, unfolding profiles for individual nucleotides were binned into eight groups (Figures 4 and 5). There is relatively little subjectivity in these assignments. First, calculated T_ms have uncertainties that are ±1 °C or less at most positions. Second, nucleotides binned into groups by T_m alone are located adjacent to each other in tRNA^{Asp}, suggesting that the binning process reports authentic independently folding regions in the RNA (Figure 5).

At 35 °C, SHAPE accurately reports the canonical structure[13] of tRNA^{Asp} (summarized in Figure 7A). Nucleotides in the T-, D-, and anticodon loops and in the 3′-CCA region are reactive, whereas nucleotides involved in base pairing and tertiary interactions are unreactive. The anticodon stem is the least constrained of the four conserved paired regions, and nucleotides in or adjacent to the G−U pair in this stem are also reactive (red nucleotides in Figure 7A).

Two-Phase Loss of Tertiary Interactions for tRNA^{Asp}. The first unfolding transition ($T_m \sim$ 51 °C) involves disruption of the tertiary interactions that link the D- and T-loops (in orange, Figure 7B). In addition, nucleotides A9−U13, which span one strand of the D-stem, become flexible in this transition. U55−A57 and U59 in the T-loop and nucleotides A14−G17 in the D loop were moderately reactive at 35 °C and become more reactive over this temperature range. We infer that these positions are moderately flexible in the native ground state and are cooperatively disrupted in this transition.

The second transition ($T_m \sim$ 53 °C) involves complete unfolding of the D-stem, coupled with disruption of the tertiary interactions between the purine-rich strand (positions G22−U25) of this stem and nucleotides U8, A21, G45, and A46 (green positions in Figure 7C). In addition, nucleotides that comprise the stacked junction between the T- and acceptor stems (G6, A7, and C49) become flexible in this transition. Inspection of the melting profiles makes clear that the 51 and 53 °C transitions are distinct (Figure 4G,H). The 51 and 53 °C transitions are also detected independently in the absorbance melting experiment (Figure 6).

An unanticipated result is thus that the purine- and pyrimidine-rich strands of the D-stem become conformationally flexible in an asymmetric way, and average T_ms are 53 and 51 °C, respectively. Only the pyrimidine-rich strand (nucleotides G10−U13) becomes unconstrained in the first transition and in concert with the T- and D-loops, as judged by SHAPE chemistry (illustrated by removal of base-pair symbols at orange nucleotides in Figure 7B). The purine strand melts with most of the tertiary interactions in this region at 53 °C (green symbols, Figure 7C). The asymmetric stability of the purine versus pyrimidine strands of the D-stem likely reflects two local structural differences. First, purine nucleotides may be better able to maintain internucleotide stacking interactions in the absence of base pairing. Second, the purine-rich side participates
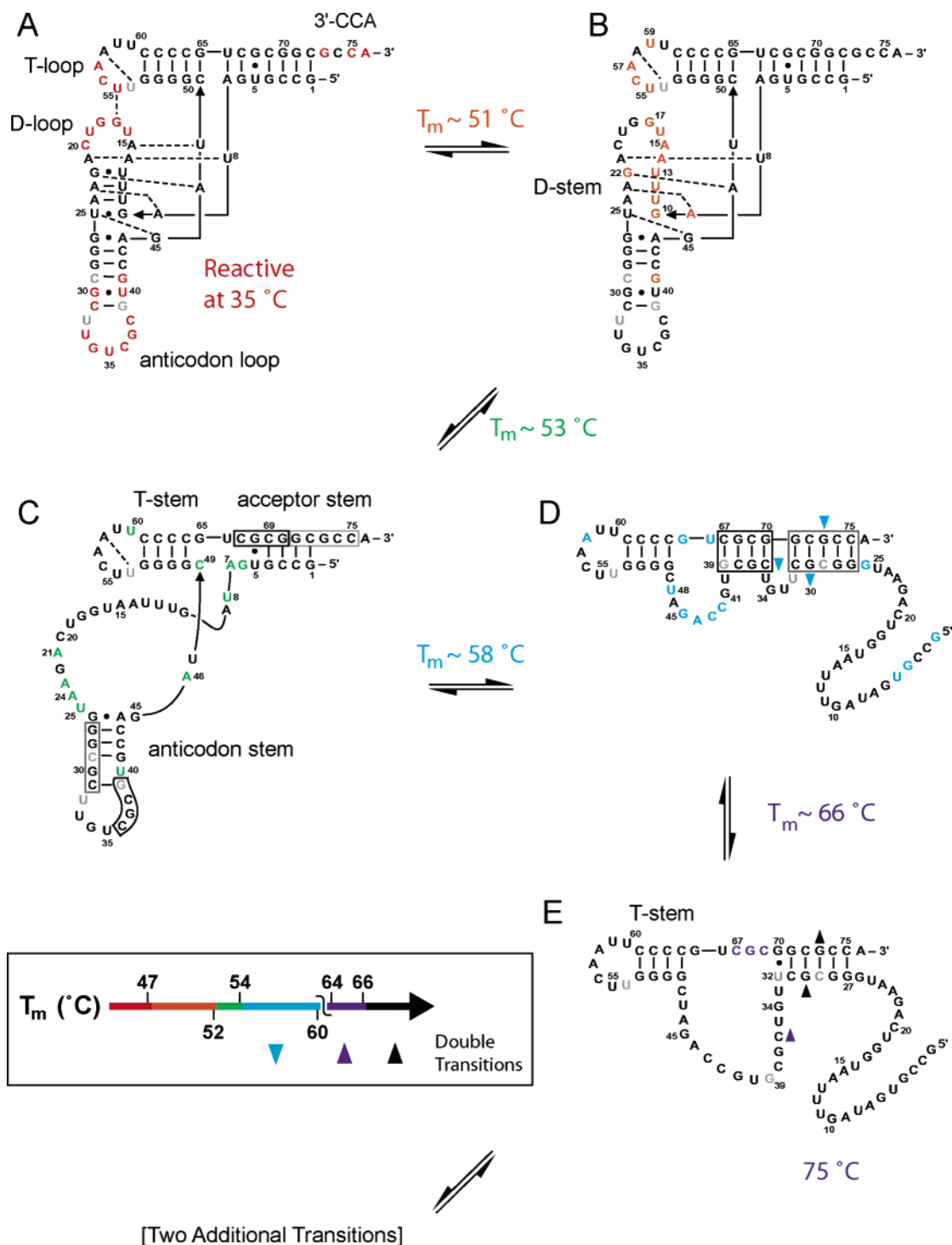
Figure 7. Nucleotide resolution model for thermal denaturation of tRNA^Asp. For each structure or intermediate (A–E), nucleotides that become newly reactive in a given transition are shown in color. Gray and black boxes (C and D) identify nucleotides proposed to participate in a conformational shift that maximizes G–C pairings. Up and down arrowheads emphasize positions that show two-phase behavior (see Figure 4C) and whose reactivity increases or decreases, respectively, in the indicated transition. Two additional transitions with T_ms ≥ 70 °C, involving disruption of the G27–U32/G70–C75 helix and the T-stem helix, are not shown.

in significant tertiary interactions with other parts of the tRNA (dashed lines in Figure 7B).

A Conformational Switch Involving the Anticodon and Acceptor Stems. In the next well isolated transition (T_m ∼ 58 °C), both the anticodon and acceptor stems unfold *asymmetrically*. One strand of each helix unfolds ≥7 °C higher than the other (compare T_ms in blue with other symbols in Figure 5). In addition, over this same temperature range, positions G30, C36,

and G73 exhibit significant *decreases* in reactivity (Figure 4C, diamonds in Figure 5), and thus structural constraints *increase* at these well-defined positions in the RNA (emphasized with blue downward arrowheads in Figure 7D).

These two, distinct observations are well explained if nucleotides on one side of each of the anticodon and acceptor stems (emphasized with gray and black boxes, Figure 7C) undergo a conformational shift to form new G–C-rich helices (gray and

black boxes, Figure 7D). Thus, as one side of the acceptor and anticodon stems becomes locally flexible and reactive toward NMIA, the other side forms new constraining base pairs with complementary sequences in the RNA. This new structure (Figure 7D) is favored at higher temperatures because the absence of native tertiary interactions that would otherwise enforce the canonical tRNA fold (see Figure 7A) changes the minimum energy structure. Alternatively, the conformational shift may reflect, in part, a temperature-dependent change in ΔH for these secondary structure motifs.

Nucleotides G37, C38, C74, and C75 likely also participate in the new helices. These nucleotides are partially reactive, at ~10−50% of the rate of the fully reactive A76 position, over the entire temperature range (Figure 3). We interpret this conserved, intermediate reactivity to indicate that these nucleotides experience a series of stacking and base-pairing constraining interactions throughout the temperature range.

Ultimate Stages of Unfolding in Three Incremental Steps. With increasing temperature, the helices formed as a result of the conformational shift (Figure 7D) then unfold incrementally and in an order consistent with calculated thermodynamic parameters.[17,18] The short helix spanning G36−G39 and C67−G70 unfolds with a T_m of ~66 °C (magenta positions in Figure 7E). The stem comprised of G27−U32 and G70−C75 unfolds next because most of these nucleotides begin to react with NMIA by 75 °C (Figure 4D, illustrated with black arrowheads in Figure 7E). Finally, the C−G-rich T-stem unfolds with a T_m that must be significantly higher than 75 °C, consistent with the observation that no detectable change in reactivity occurs at these positions through 75 °C (Figure 4A; summarized with solid stars in Figure 5).

Implications for the RNA Folding Problem. The single nucleotide resolution SHAPE analysis illustrates a complexity in folding states for tRNA^{Asp} transcripts that is not anticipated by current models for RNA folding. First, RNA folding is thought to be strongly hierarchical such that the base-paired secondary structure is more stable than and forms independently of tertiary interactions. For the tRNA^{Asp} construct, this model is clearly only partially predictive. It is true that the two lowest temperature transitions, at 51 and 53 °C, both involve loss of tertiary interactions. However, in both cases, disruption of tertiary structure is coupled with the loss of simpler base-paired interactions (see Figure 7B,C). This coupling is so tight that the base-paired D-stem is better viewed as an obligate component of the tRNA tertiary structure.

Second, the structural stability of an individual helix is usually approximated to be uncoupled from the structure of other helices, with the exception of end-stacking effects.[18,19] However, for tRNA^{Asp}, there are two distinct examples in which the two strands in an RNA helix unfold asymmetrically due to structural coupling with other parts of the molecule. In the first example, the purine-rich strand of the D-stem becomes conformationally flexible at a temperature higher than that of the pyrimidine-rich strand of the same helix due to the influence of the tRNA tertiary structure (see Figure 7B,C). Second, both the anticodon and acceptor stems melt asymmetrically, consistent with a conformational switch (Figure 7C,D) in which the partially denatured tRNA refolds to an alternate three-helix structure at elevated temperature.

Facile Analysis of RNA Folding Pathways. SHAPE chemistry makes possible quantitative analysis of RNA base pairing and tertiary interactions at single nucleotide resolution. Because NMIA reacts at the 2′-hydroxyl position, all nucleotides are interrogated and the *absence* of reactivity can be confidently assigned to persistent stability at a given local structure. The fundamental conclusion of this work is that, even for relatively simple tRNA^{Asp} transcripts, the equilibrium conformational states most structurally accessible from the native state are not well predicted by the hierarchical model for RNA folding. We are hopeful that the comprehensive and quantitative view of RNA structure afforded by the SHAPE approach will provide the experimental framework necessary for understanding the interrelationships between local and higher order folding in RNA.

Experimental Section

General. The tRNA^{Asp} transcript was synthesized by in vitro transcription in the context of a structure cassette containing flanking 5′ and 3′ sequences (Figure 2) to facilitate analysis of the entire RNA by primer extension.[7] The RNA was purified by denaturing electrophoresis and stored in 10 mM Na/Hepes (pH 8.0) and 1 mM EDTA.

Temperature Dependence of NMIA Hydrolysis and 2′-Ester Formation. NMIA degradation by hydrolysis was followed by adding (1 μL, 10 mM) reagent to buffer [2 mL, 100 mM potassium phosphate (pH 8), 250 mM NaCl, 10% v/v DMSO] equilibrated (at 15, 25, 35, 45, or 55 °C) in a fluorescence cuvette. Pseudo-first-order rates were obtained by monitoring formation of the fluorescent hydrolysis product, 2-methylaminobenzoate (excitation and emission at 375 and 440 nm, respectively). Rates of adduct formation for the [^{32}P]-labeled nucleotides, ATP, pAp, pAp-ethyl, and 2′-deoxy-ATP, were obtained by adding NMIA (in DMSO), quenching the reaction with 1 vol 250 mM dithiothreitol, and visualizing reaction products by gel electrophoresis.[7] Once the rate of NMIA hydrolysis ($k_{hydrolysis}$) was determined for a given temperature, rates for 2′-O-adduct formation (k_{adduct}) were obtained by fitting to: fraction product = $1 - \exp[(k_{adduct}/k_{hydrolysis})(e^{-k_{hydrolysis}t} - 1)]$. Product formation is pseudo-first-order in both hydrolysis and NMIA concentration and will be independent of RNA concentration through ~1 mM.

Temperature-Dependent RNA Modification. RNA (6 μL, 20 pmol, in ~2 mM Hepes, pH 7.5) was heated at 95 °C for 3 min, cooled on ice, treated with 3 μL of folding buffer [333 mM NaCl, 333 mM Hepes (pH 8.0), and 33.3 mM MgCl$_2$], and incubated at 37 °C for 20 min. The RNA solution was then equilibrated for 5 min at the reaction temperature (35−75 °C), treated with NMIA (Molecular Probes; 1 μL, 130 mM in anhydrous DMSO), allowed to react for five hydrolysis half-lives (54−1.2 min for 35−75 °C, respectively), and placed on ice. No NMIA controls and prequench reactions were performed by substituting DMSO alone for NMIA or by allowing the NMIA to degrade prior to addition of RNA, respectively. Temperature gradient was established using an Eppendorf gradient thermocycler using 45 ± 10 and 65 ± 10 °C gradient settings; temperatures used were 34.9, 36.3, 38.0, 40.3, 42.9, 45.7, 48.4, 51.0, 53.2, 54.8, 58.3, 60.6, 63.2, 65.9, 68.5, 71.0, 73.1, and 75.4 °C (see Figure 3). Efficiency of 2′-O-adduct formation was obtained from primer extension reactions, performed exactly as described[7] and resolved on (8%) denaturing polyacrylamide gels.

(17) (a) Jaeger, J. A.; Turner, D. H.; Zuker, M. *Methods Enzymol.* **1990**, *183*, 281−306. (b) Xia, T.; SantaLucia, J. J.; Burkard, M. E.; Kierzek, R.; Schroeder, S. J.; Jiao, X.; Cox, C.; Turner, D. H. *Biochemistry* **1998**, *37*, 14719−14735.

(18) Mathews, D. H.; Disney, M. D.; Childs, J. L.; Schroeder, S. J.; Zuker, M.; Turner, D. H. *Proc. Natl. Acad. Sci. U.S.A.* **2004**, *101*, 7287−7292.

(19) (a) Walter, A. E.; Turner, D. H.; Kim, J.; Lyttle, M. H.; Muller, P.; Mathews, D. H.; Zuker, M. *Proc. Natl. Acad. Sci. U.S.A.* **1994**, *91*, 9218−9222. (b) Draper, D. E.; Gluick, T. C. *Methods Enzymol.* **1995**, *259*, 281−305.

Quantification of RNA Reactivity. The gel image was quantified by phosphorimaging and band intensities integrated using SAFA.[20] Nucleotide reactivities were normalized to a uniformly reactive position (G18 for nucleotides G1−C49; A76 for G50−C75); absolute reactivities typically increased 5−8-fold for nucleotides that showed well-defined melting transitions. Data obtained as a function of temperature at individual nucleotides were rescaled to a unit (0→1) scale and smoothed using a rolling weighting function.[21] Transition midpoints (T_m) were obtained assuming a unimolecular transition:[22]

$$I = A\frac{1}{1 + \left[\exp\left[\frac{\Delta H_{vH}}{R}\left(\frac{1}{T_m} - \frac{1}{T}\right)\right]\right]^{-1}} + b$$

where I is the band intensity at a given temperature (T); R is the gas constant, and A and b are the transition amplitude and initial intensity, respectively. The van't Hoff enthalpy (ΔH_{vH}) is returned by this equation but is characterized by large fitting errors. In contrast, melting temperatures are generally (34 of 41 positions) reproducible to ±1 °C

or better. Error limits for nucleotides U11, U16, G65, C67, and G68 are ±2 °C and for U40 and C43 are ±3 °C.

Monitoring RNA Denaturation by UV Absorbance. The tRNA^Asp construct (5 μM, 600 μL) was heated from 35 to 90 °C in an Applied Photophysics Pistar-180 spectrometer at 1 °C/min under exactly the conditions used in the SHAPE experiments (including DMSO, but omitting NMIA). After subtracting background from a sample omitting RNA, the denaturation profile, monitored at 260 nm, was smoothed[21] and algebraically differentiated with respect to temperature.

(20) Das, R.; Laederach, A.; Pearlman, S.; Herschlag, D.; Altman, R. B. SAFA: Semi-automated Footprinting Analysis Software for High-Throughput Quantification of Nucleic Acid Footprinting Experiments. *RNA* **2005**, *11*, 344−354.

(21) Chambers, J. M.; Cleveland, W. S.; Kleiner, B.; Tukey, P. A. *Graphical Methods for Data Analysis*; Wadsworth International Group: Belmont, CA, 1983; pp 91−104.

(22) John, D. M.; Weeks, K. M. *Protein Sci.* **2000**, *9*, 1416−1419.